frontiers | Frontiers in Astronomy and Space Sciences

TYPE Original Research
PUBLISHED 20 February 2023
DOI 10.3389/fspas.2023.1108386

OPEN ACCESS

EDITED BY
Francesca Altieri,
Institute for Space Astrophysics and Planetology (INAF), Italy

REVIEWED BY
Jianguo Yan,
Wuhan University, China
Gwénaël Caravaca,
UMR5277 Institut de recherche en astrophysique et planétologie (IRAP), France

*CORRESPONDENCE
G. Schmidt,
genewalter.schmidt@uniroma3.it

SPECIALTY SECTION
This article was submitted to Planetary Science,
a section of the journal
Frontiers in Astronomy and Space Sciences

RECEIVED 26 November 2022
ACCEPTED 07 February 2023
PUBLISHED 20 February 2023

CITATION
Schmidt G, Luzzi E, Franchi F, Selepeng AT, Hlabano K and Salvini F (2023), Structural influences on groundwater circulation in the Makgadikgadi salt pans of Botswana? Implications for martian playa environments.
Front. Astron. Space Sci. 10:1108386.
doi: 10.3389/fspas.2023.1108386

Structural influences on groundwater circulation in the Makgadikgadi salt pans of Botswana? Implications for martian playa environments

G. Schmidt[1]*, E. Luzzi[2,3], F. Franchi[4], A. T. Selepeng[4], K. Hlabano[4] and F. Salvini[1]

[1]Laboratorio di Geodinamica Quantitativa e Telerilevamento (GeoQuTe), Department of Science, Università Degli Studi Roma Tre, Rome, Italy, [2]Bay Area Environmental Research Institute (BAERI), NASA Ames Research Center, Moffett Field, CA, United States, [3]Department of Physics and Earth Sciences, Jacobs University Bremen, Bremen, Germany, [4]Earth and Environmental Science Department, Botswana International University of Science and Technology, Palapye, Botswana

Across the surface of Mars, evidence of past lacustrine and evaporitic environments has been found within basins and craters, where often layered sedimentary deposits and hydrated minerals are observed. However, the intensity, duration, and precise phases of aqueous processes during their deposition remain unresolved mostly for our inability to model subsurface structures. Although several geological processes and locations on Earth have been previously proposed as examples to describe these deposits on Mars, we lack a strong visualization of what water activity might have looked like during evaporitic stages within basins and craters. Here we propose to investigate the shallow subsurface of the Makgadikgadi salt pans of Botswana as a potential analog for understanding groundwater upwelling on Mars. The pans are found within the Makgadikgadi Basin, a depression located at the southwestern end of a northeast-southwest set of graben linked with the East African Rift. The Makgadikgadi Pans are evaporitic environment rich in hydrated minerals and groundwater activity. The purpose of this work is to identify buried faults and areas of relative water saturation within the lacustrine sediment of the Makgadikgadi Basin by means of electrical resistivity surveys. This work represents the first electrical resistivity survey of the basin floor which provides a precursory investigation of the relationship between groundwater, faults, basement depth, and the lacustrine sediments. We present four electrical survey lines from different locations in the pans which reveal distinct sedimentary units. Several faults are inferred from the vertical displacement of these units and accompanying low resistivity where displacement is observed. These results provide a framework for visualizing the sedimentary sequences of infilled basins and craters on Mars, which can broaden the ongoing discussion of hydrogeological processes that were active in the planet's past. We propose Meridiani Planum, as well as Oyama and Becquerel crater of Arabia Terra as locations to establish this framework. Since such processes are still ongoing in the Makgadikgadi Basin, imaging the subsurface of the pans helps explain the formation of layered and salty deposits on the surface of Mars, how they may have interacted with flowing water, and whether they might have hosted life.

KEYWORDS

playa deposits, ephemeral lake, evaporites, electrical resistivity, mars sediments, mars groundwater

1 Introduction

The presence of sedimentary rocks and past aqueous depositional environments on Mars have been substantiated by both orbital and surface instrumentation (e.g., Lucchitta et al., 1994; Squyres et al., 2004; Fueten et al., 2005; Haskin et al., 2005; Pondrelli et al., 2008; Carr and Head, 2010; Le Deit et al., 2013; Le Deit et al., 2016; Salese et al., 2019; Salese et al., 2020; Mangold et al., 2021; Changela et al., 2022). One of the past Martian environments where water is thought to have played a fundamental role is known as a playa. A playa is characterized by a depressed basin where cycles of flowing water and evaporation are observed. The evaporation leads to the formation of hydrated sulfates (e.g., gypsum, halite, epsomite, and kieserite), chlorides, and hydrated silica (i.e., opal), which together with clays (e.g., kaolinite, smectite, and illite) constitute the characteristic mineralogical assemblage found within playas (Crowley, 1993; Drake, 1995; Viviano et al., 2014; Wang et al., 2016). The water input in playas can be provided mainly by two sources: surface runoff or groundwater flows (McKenna and Sala, 2018). Playa environments predominantly fed by groundwater are often rich in evaporite crusts (Nield et al., 2016).

There are currently two radar instruments in Martian orbit, the Mars Advanced Radar for Subsurface and Ionospheric Sounding (MARSIS) on Mars Express (Jordan et al., 2009) and the Shallow Radar (SHARAD) on the Mars Reconnaissance Orbiter (MRO) (Seu et al., 2007; Zurek and Smrekar, 2007), both capable of detecting groundwater on Mars. Although neither instrument has been able to confirm shallow groundwater on Mars, this non-detection, possibly caused by the high conductivity of the Martian crust, is not necessarily ruling out the presence of such a body of water (Farrell et al., 2009; Nunes et al., 2010; Abotalib and Heggy, 2019). A deep aquifer (depth >1.5 km) was inferred in the polar region using MARSIS (Orosei et al., 2018), which opened up theories catering to the presence of deep groundwater elsewhere on Mars. Although the presence and specific characteristics of any deep aquifer is still an ongoing debate (Sori and Bramson, 2019; Bierson et al., 2021), the possibility of their existence is intriguing due to the protection from solar radiation such depths would provide for microbial life. Regardless, in spite of unequivocal evidence for extant groundwater on Mars are sparse, there are abundant geological clues that point toward a warmer and wetter planet with a complex hydrogeological history (e.g., Carr and Head, 2010; Di Achille and Hynek, 2010; Orofino et al., 2018; Salese et al., 2019; Dickeson and Davis, 2020; Dickeson and Davis, 2020; Fawdon et al., 2022; Michalski et al., 2022; Schmidt et al., 2022).

Several areas on Mars have been interpreted as playa environments based mainly on the occurrence of sulfates/chlorides (e.g., Wang et al., 2016) and/or morphological evidence for aqueous activity (e.g., Franchi et al., 2014; Pondrelli et al., 2015). Some of the areas where the playa environment has been identified, including Meridiani Planum (Grotzinger et al., 2005; Andrews-Hanna et al., 2010) and Arabia Terra (Franchi et al., 2014; Pondrelli et al., 2015; Pozzobon et al., 2019), occur within a regional paleo-hydrological system characterized by groundwater upwelling (see global model in Andrews-Hanna et al., 2007). Polygonal (desiccation) cracks and occurrence of chlorides in association with smectite in playa-like settings across Mars are other indirect evidencefor the existence of large ephemeral lakes that led to the deposition of lacustrine and interbedded evaporitic deposits within topographical lows and basins (e.g., El Maarry et al., 2013; Nachon et al., 2014; Rapin et al., 2016; Stein et al., 2018; Caravaca et al., 2021; Caravaca et al., 2022).

The interpretation of the aforementioned Martian regions as playa environments is not without controversies, especially when direct observation for the global groundwater system is missing. Hence, the study of terrestrial playa environments such as the Makgadikgadi of Botswana becomes crucial. The Makgadikgadi Basin in northcentral Botswana, Africa (Figure 1A) is the relict of a mega-lake system, known as Lake Paleo-Makgadikgadi (Grey and Cooke, 1977; Thomas and Shaw, 1991; Burrough et al., 2009; Podgorski et al., 2013; Riedel et al., 2014; Schmidt et al., 2017; Franchi et al., 2022) and it has been considered as a potential analogue of some of the Equatorial Layered Deposits (ELDs) formed within Martian evaporitic environments (Franchi et al., 2020). This lacustrine system formed in the Early Pleistocene by the uplift of the Chobe Fault as part of the South-Western migration of the East Africa Rift (EAR) (e.g., Moore et al., 2012). Since the Pleistocene, the evolution of the Makgadikgadi Basin has been driven by faults and tectonic events linked to the EAR system (e.g., Schmidt et al., 2023). These tectonic events shaped the river watersheds and regulated the sources of surface water inflow into the basin (Moore et al., 2012; Riedel et al., 2014). The basin has undergone at least four highstand phases during the last 40 ka and a prolonged dry period initiated ca. 17 ka and culminated in the present-day conditions of playa lake (Burrough et al., 2009; Franchi et al., 2022). The Makgadikgadi Basin consists of a system of playa lakes (hereafter referred to as Makgadikgadi Pans) including the Ntwetwe Pan in the west and the Sua Pan in the east (Figure 1B). Today, the Makgadikgadi Pans receive seasonal surface water from ephemeral rivers flowing from the east and north-east, and seasonally by the Boteti River in the south-west. Nevertheless, previous authors have postulated that the role of groundwater upwelling in the pan lowlands must be a crucial morphological factor and contributes to the overall water balance of the Makgadikgadi (McFarlane and Long, 2015; Franchi et al., 2020). Franchi et al. (2020) also demonstrated that the presence of layered mounds within the interior of the pans could be related to groundwater fluctuations and changes in water saturation within the capillary fringe, resulting in preferential erosion. Nevertheless, it is still disputed precisely how the groundwater upwelling is affecting the evolution of the pans (e.g., Richards et al., 2021).

Here electrical resistivity methods are applied for imaging fault lines previously identified with airborne geophysics and buried under lacustrine sediments to generate 2D Electrical Resistivity Tomography (ERT). This method allows the detection of changes in relative electrical resistance within void space produced by any faults and associated fractures in the overlaying water saturated sediment (Kolawole et al., 2018; Ojo et al., 2022).

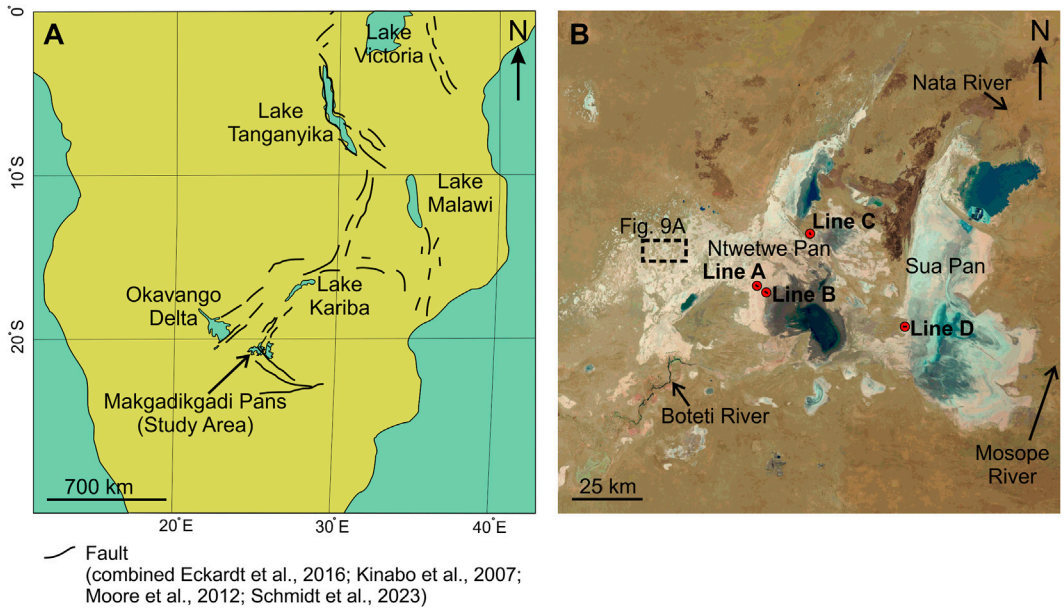

FIGURE 1
The Makgadikgadi Pans (Botswana). **(A)** Regional map of Southern Africa. Major faults are labeled with bold black lines, the majority of which are associated with the East African Rift (EAR). The Makgadikgadi Pans represent the southernmost termination of the EAR. Modified from Schmidt et al. (2023). **(B)** Landsat 8 images of the pans from October 2021 (-20.8°, 25.5°). Red circles indicate ERT survey line locations (Lines A, B, C, D).

The aim of this work is to shed light on the relationship between faults and groundwater flow in an otherwise arid, evaporitic environment by means of ERT. This data provides insights on the depth and saturation of sediments in an evaporative setting, which is bound to teach us more about the processes of formation and erosion of playa deposits on Mars, their relationships with groundwater upwelling and, eventually, if they were formed in a wetter and habitable Mars.

2 Geological setting

2.1 Makgadikgadi Basin

2.1.1 Bedrock geology

The Makgadikgadi Pans lie within a fault-bounded basin that consists of crystalline basement and the volcano-sedimentary units of the Karoo Supergroup (Eckardt et al., 2016; Schmidt et al., 2023). The Karoo Supergroup units in the area include basal Late Carboniferous glacial deposits of the Dwyka Group (Dukwi Formation in Botswana; Dietrich et al., 2019) unconformably overlain by the Carboniferous to Early Permian Ecca Group, by the Upper Permian to Lower Triassic Beaufort Group (Tlhabala Formation in Botswana; see review in Bordy, 2020) and by the Middle Triassic to the Middle Jurassic continental sandstones and mudstones of the Lebung Group (see Franchi et al., 2021 for a review). Along the northern and southern edges of the Makgadikgadi Basin, the bedrock geology is characterized by Early Jurassic (ca. 185 Ma) basalts of the Stormberg Lava Group. The Karoo Supergroup units are crossed by an ESE-WNW trending doleritic Okavango Dike Swarm, which is part of the Karoo Large Igneous Province and have been dated at ca. 187 Ma (Elburg and Goldberg, 2000).

The Makgadikgadi Basin is filled by post-Karoo sediments grouped under the Kalahari Group (Thomas and Shaw, 1991; Haddon and McCarthy, 2005). These Kalahari Group units are constituted by a sedimentary succession whereby basal conglomerates and gravels are commonly overlain by clay beds and sandstones capped by unconsolidated sands (Haddon and McCarthy, 2005). The thickness of this unit of unconsolidated sands can vary from 50 to 300 m in the Makgadikgadi Basin (Thomas and Shaw, 1991; Nash et al., 1994; Haddon and McCarthy, 2005; Ringrose et al., 2009). The sedimentary units within the Kalahari Group found within the pans are referred to as the Makgadikgadi Group in this work, following the nomenclature of available drill core data.

2.1.2 Evolution of the Makgadikgadi Basin

The Makgadikgadi Basin, that currently consists of a system of playa lakes, is situated in the central Kalahari Basin of Botswana (Figure 1) (Moore et al., 2012). This basin developed within the Makgadikgadi-Okavango-Zambezi Basin (MOZB), the South-Western branch of the EAR (e.g., Modisi et al., 2000; Kinabo et al., 2007; Ringrose et al., 2009; Riedel et al., 2014). There is still controversy concerning the age of the first mega-lake formed in the central Kalahari Basin; Burrough et al. (2009) proposed an OSL (Optical Stimulated Luminescence) age of 288 ± 25 ka for the oldest strandline (i.e., shoreline) of the Lake Paleo-Makgadikgadi. Most probably, the formation of the paleo Lake Deception, a precursor of the Lake Paleo-Makgadikgadi, begun in the Early Pleistocene (ca. 2.5 Ma) with the diversion of the paleo river Chambeshi in northern Botswana after the activation of the Chobe Fault (Moore et al., 2012). After the initial

impoundment of the basin the tectonic events through the Middle and Late Pleistocene led to a gradual contraction of the paleo lake to i) 945 m a.s.l., in the Early to Middle Pleistocene, after the uplift of the Congo-Zambezi watershed; and ii) 912 m a.s.l., after the diversion of the Upper Zambezi in the Bulozi graben (Moore et al., 2012, 0.5–5.0 m vertical error demonstrated by Mukul et al., 2017). The propagation of the EAR culminated in the Late Pleistocene, ca. 100 ka, in the activation of the Thamalakane Fault in the north west of Botswana, leading to the formation of the Okavango Delta, and causing a progressive desiccation of the Lake Paleo-Makgadikgadi (Moore et al., 2012). Between 46 ka and the Last Glacial Maximum the Makgadikgadi Basin was cyclically fed by the palaeo-Boteti and palaeo-Nata rivers and, lastly, by the Okwa River reaching the level of ca. 936 m a.s.l for the last time (e.g., Riedel et al., 2014). The evolution of the basin in the Holocene was recently unraveled by means of ostracod fauna correlation, revealing an overall desiccation trend starting with the highstand at ca. 17 ka BP, followed, at around 1.4 a, by a relative increase in the lake water level (Franchi et al., 2022). The complete desiccation of the Makgadikgadi Basin occurred in the last 1.4 ka and led to the formation of the present day Makgadikgadi Pans (Figure 1B) (Franchi et al., 2022).

2.1.3 Makgadikgadi Pans hydrology

The Makgadikgadi Pans receive seasonal surface water from ephemeral rivers flowing from the east and northeast, and seasonally by the Boteti River in the southwest (Figure 1B) (e.g., Franchi et al., 2020). The basin receives relatively low mean annual rainfall (~300 mm yr^{-1}) with precipitation limited to the summer season (Burrough et al., 2009). Both Ntwetwe and Sua pans are cyclically inundated during the short, wet season between November and March (e.g., McCulloch et al., 2008). These fluctuations over the wet and dry seasons contribute to the formation of brines and consequent deposition of evaporite minerals and clays on the pan floor (Eckardt et al., 2008; Ringrose et al., 2009). Wind erosion and calcretisation are the dominant process during the dry, winter season (Nash et al., 1994; Riedel et al., 2014).

Several authors suggested that to justify the water budget in the basin and the existence of some peculiar morphologies (i.e., layered mounds) the existence of groundwater upwelling must be factored in (e.g., MacFarlane and Long, 2015; Franchi et al., 2020). MacFarlane and Long. (2015) suggested that layered mounds within the Ntwetwe Pan are spring mounds produced by groundwater discharge along the gradient of the shoreline. Areas of this shoreline have been suggested to be a fault scarp (Eckardt et al., 2016; Schmidt et al., 2023 IN PRESS). Groundwater movement into the pans has been modeled previously and demonstrated to be largely attributed three large aquifers, the Lebung, Ecca, and Ghanzi, which share regional flow patterns directed into the pans (Lekula et al., 2018). However, the implications of groundwater movement on the evaporation rates and surface moisture are still poorly understood in the pans (Nield et al., 2016).

2.2 Martian environments

2.2.1 Playa lakes on mars

A variety of locations on Mars have been identified as likely representing lacustrine environments (Cadieux and Kah, 2015; Day and Catling, 2020; Lucchitta et al., 1994, Lucchitta, 2010; Schmidt et al., 2022). The majority of these environments are thought to have been sustained in the Late Noachian (>3.7 Ga), with many occurring in the Hesperian (3–3.7 Ga) and some possibly as late as the Amazonian (<3 Ga) (Michalski et al., 2022). These eventually developed into evaporitic environments as consequence of a global drying process (Allen and Oehler, 2008; Al-Samir et al., 2017; Allen and Oehler, 2008; Andrews-Hanna et al., 2010; Franchi et al., 2014; Pondrelli et al., 2015; 2019; Schmidt et al., 2018; Pozzobon et al., 2019; Rossi et al., 2008). These evaporitic deposits formed during the Hesperian and possibly the Early Amazonian (Flahaut et al., 2017; Leask and Ehlmann, 2022) following periods of oscillating water tables (Andrews-Hanna et al., 2007; 2010; Schmidt et al., 2021; 2022). The evaporitic environments on Mars are often located within basins and craters which are filled with several hundred meters of sediment, often covering the entire crater floor (Franchi et al., 2014; Pondrelli et al., 2019; Schmidt et al., 2021). The existence of conical mounds on the top surface of these sedimentary sequences has been broadly documented (e.g., Allen and Oehler, 2008; Franchi et al., 2014; Pondrelli et al., 2015; 2019; Rossi et al., 2008). The formation of these mounds has been proposed to be the result of spring activity along faults (Allen and Oehler, 2008), hydrothermal activity (Pondrelli et al., 2015), or differences in water saturation which creates a preferential erosion phenomenon (Franchi et al., 2020). Furthermore, subsurface fluid pressure has been

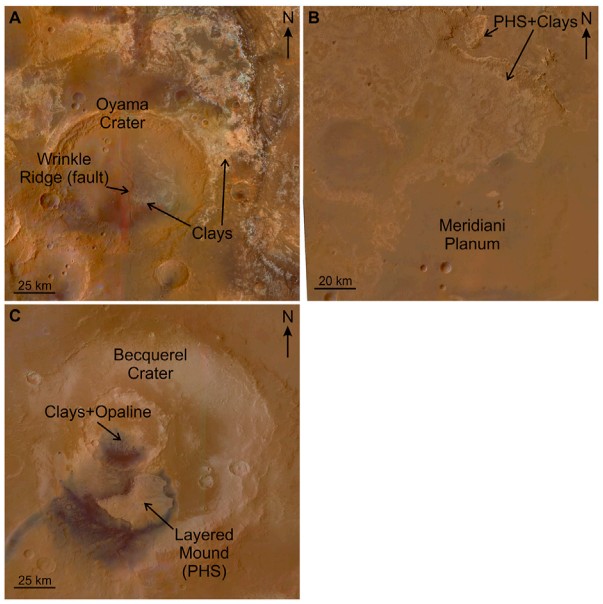

FIGURE 2
Several locations within Arabia Terra (Mars) that share various similarities to the Makgadikgadi Pans (Botswana). **(A)** HRSC colorized mosaic of Oyama crater (23.5°, -20.1°) with the central wrinkle ridge and regions of clays (Loizeau et al., 2012; Loizeau et al., 2015; Tanaka et al., 2014). **(B)** HRSC colorized mosaic of Meridiani Planum (-0.8°, 0.9°) with areas of hydrated minerals indicated (Flahaut et al., 2015). **(C)** HRSC colorized mosaic of Becquerel crater (-8.0°, 21.5°) with areas of hydrated minerals indicated (Schmidt et al., 2022).

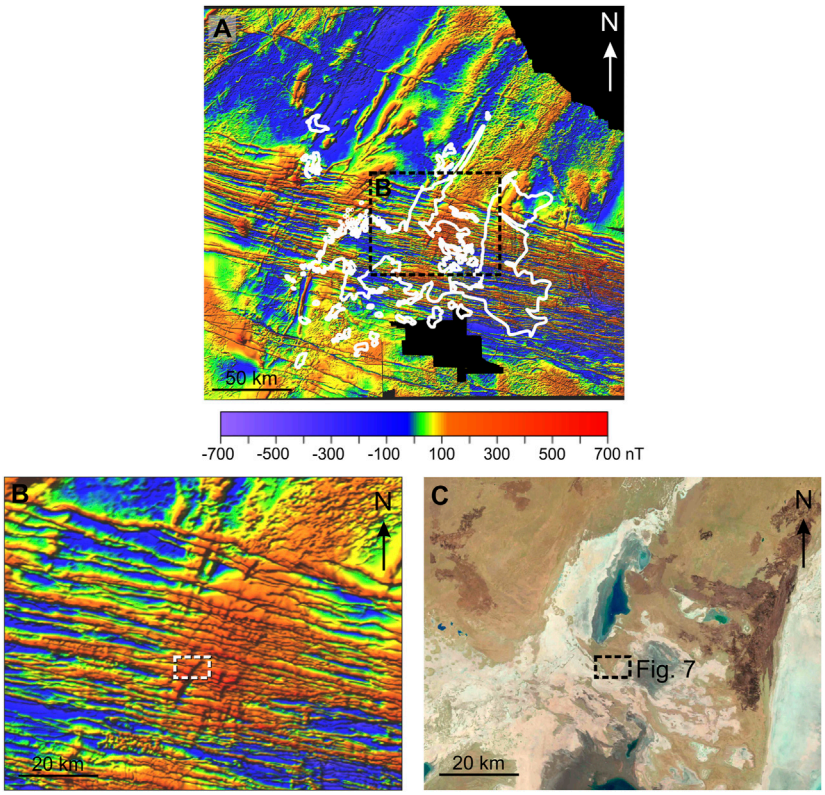

FIGURE 3
(A) Total magnetic intensity map derived from aeromagnetic data. The Makgadikgadi Pans are outlines in white. **(B)** Close-up of the magnetic intensity showing linear buried strucutres in the are of the northern Ntwetwe Pan. **(C)** Accompanying Landsat 8 image. Dashed box marks the location of Figure 7.

demonstrated to have been a reoccurring force acting on the sediments within Gale crater (De Toffoli et al., 2020), a crater which has been previously proposed to be a lacustrine environment (Grotzinger et al., 2005; Achilles, et al., 2020) which later developed into an evaporitic setting (Hurowitz et al., 2017; Kah et al., 2018).

Arabia Terra has abundant sedimentary deposits, often associated with clays and hydrated sulfates (e.g., Loizeau et al., 2012; Loizeau et al., 2015; Schmidt et al., 2022), which are thought to be representative of evaporitic environments (e.g., Wang et al., 2016). We propose that the Makgadikgadi Pans are analogous to several specific locations within the region (Figure 2). Oyama crater (Figure 2A) is unique due to a large N-S striking fault that cuts across it. On the hangingwall surface of the fault, in the center of Oyama, clay mineral signatures were identified (Loizeau et al., 2012; Loizeau et al., 2015). Becquerel crater (Figure 2C) was proposed to have had a protracted water level due in part to discharged water from buried faults, and also has clay and hydrated sulfate mineral signatures (Schmidt et al., 2022). Southwest from Arabia Terra (Figure 2B), Meridiani Planum was proposed to have been the site of extensive fluid expulsion (Andrew-Hanna et al., 2010). This is the region where the Opportunity rover found hydrated minerals (Christensen et al., 2004) and where abundant hydrated sulfates and clay signatures were identified (Flahaut et al., 2015).

3 Materials and methods

3.1 Field work

Field work took place in October 2021 as part of Europlanet transnational access program. In preparation for the field work, specific areas of interest were selected within the Makgadikgadi Pans using a combination of aeromagnetic and topographic data. Topographic data were combined with a colorized mapping of slope directions and curvature to pinpoint fault scarps following the method described in Schmidt et al. (2023). Within the GIS environment Surfer® v22 (Golden Software, LLC), we processed aeromagnetic data to create a total magnetic intensity map to locate buried structures (Figure 3) (Schmidt et al., 2023). Four locations were selected for conducting the ERT survey (Figure 1B, Figure 4). These areas were selected also based on accessibility, feasibility, and spatial relationship to the inferred faults. The ERT survey lines (Figure 1B, Figure 4, Figure 5) were arranged perpendicular to the fault scarps identified by Eckardt et al. (2016); Schmidt et al. (2023), as well as magnetic structures identified in Figure 3, to ensure that the returned 2D ERT would potentially cross the faults.

Shallow subsurface geoelectrical imaging was carried out using the ERT technique to study the heterogeneity of the subsurface based on the resistance of the material to the induced electrical current artificially injected on the ground (Sudha et al., 2009). One 840 m (Line C) and three 1,200 m long survey lines (Lines A, B, and D) were successfully

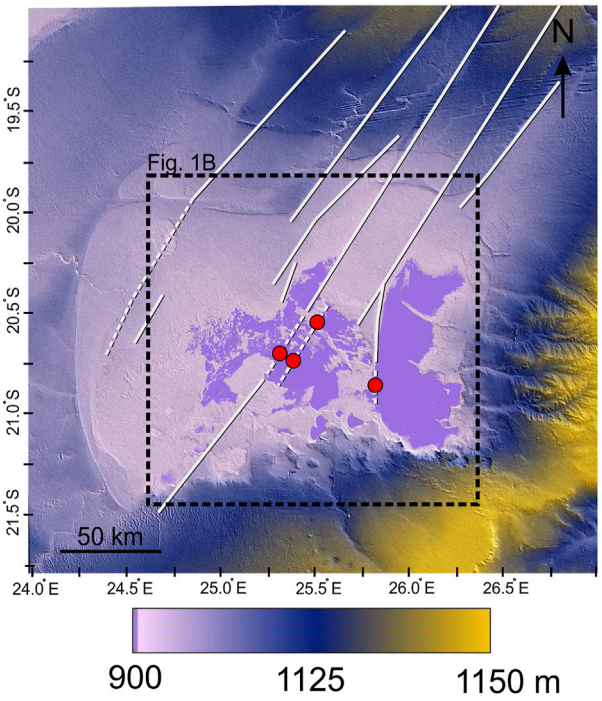

FIGURE 4
Topographic data of the Makgadikgadi Basin for regional context and fault identification. White lines mark fault locations. Dashed sections indicate inferred position of faults underneath pan sediment. Red circles mark the location of the four ERT survey lines. Modified from Schmidt et al. (2023).

laid using an IRIS Syscal Pro imaging resistivity meter available at Botswana International University of Science and Technology (BIUST) (Figure 5; Figure 6; Figure 8). The IRIS Syscal Pro is a 48 channel resistivity meter programmed to acquire data on the dipole-dipole array configuration to produce high resolution 2-D sections of the subsurface. Each survey required the initial laying of 480 m of electric cable and 48 electrodes (spaced at 10 m intervals) to retrieve the initial dataset of the survey line. The control unit at the center of the 480 m spread was powered by a 12 V battery. After the data collection along the initial 480 m, the survey proceeded following a roll-along technique whereby the first 120 m of line were disassembled and connected at the end of the initial 480 m line (Loke, 2001). This process was repeated six times for each line until the total length of 1,200 m was reached. The only exception was for Line C, where surface conditions did not allow continuing passed 840 m (Figure 7). This processes yielded an average exploration depth of 100–120 m. Each electrode had to be carefully catalogued with a differential GPS to ensure the reconstruction of a detailed topographic model for the 2D ERT profiles.

3.2 Data processing and remote sensing

3.2.1 Survey line processing

To achieve a 2-D resistivity model of the subsurface, the data were preliminary processed using PROSYS II software to eliminate bad data points and constrain the apparent resistivity values. The resulting apparent resistivity data were then inverted using the RES2DINV (ver. 3.59; Loke, 2001) which uses a least-squares smoothness constrained approach to produce a 2D resistivity model with lateral vertical

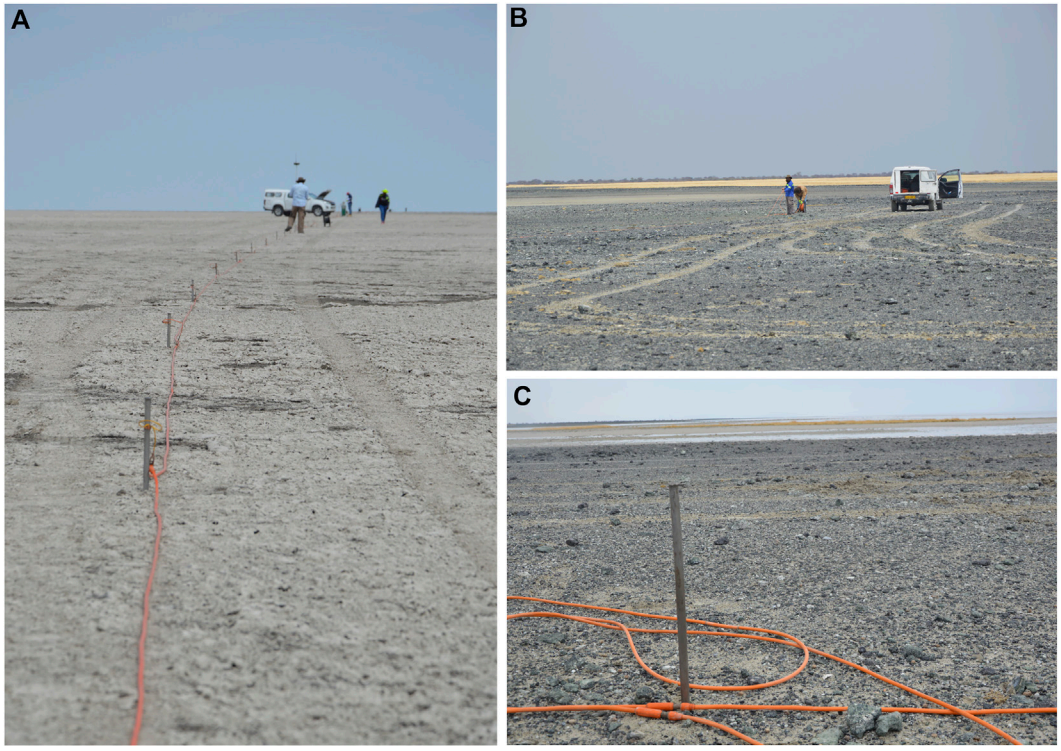

FIGURE 5
Ground views of the cable and electrodes along Line A **(A)** and Line D **(B, C)**. C) Water in the background.

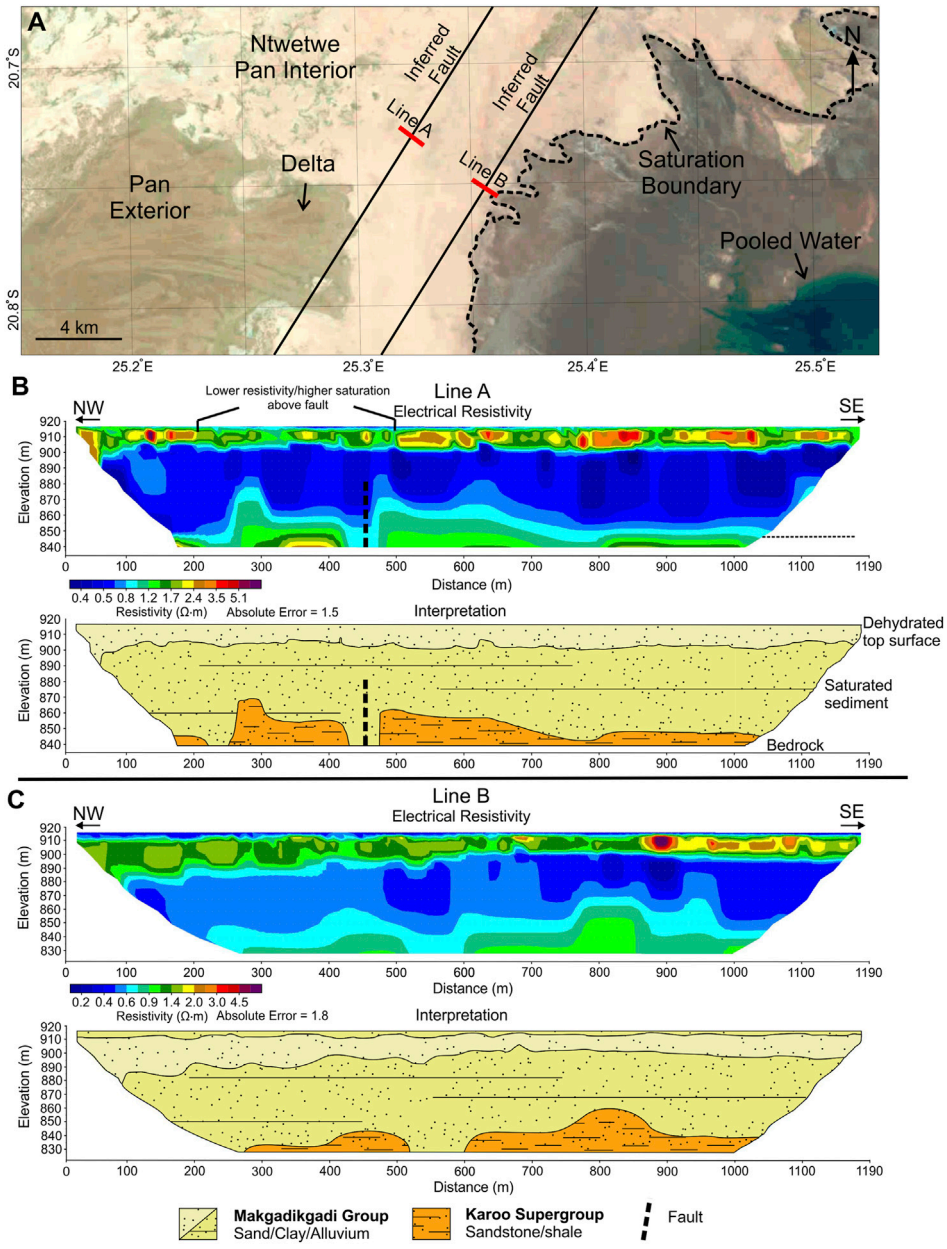

FIGURE 6
ERT survey lines **(A)**, **(B)**. **(A)** Landsat-8 image from September 2021 marking the location of ERT survey lines A and B within the Ntwetwe Pan. Pooled water can be observed in the southeast corner. A relict delta can be observed just southwest of the survey lines (Franchi et al., 2020). **(B)** Profile of ERT survey line A and interpretation showing the likely lithostratigraphic units in the subsurface. **(C)** Profile of ERT survey line B and stratigraphic interpretation.

contoured variation (deGroot-Hedlin and Constable, 1990; Loke and Barker, 1996). The 2-D models from the inversion software were then used to interpret the subsurface conditions.

Drill core data from exploration companies (Falconbridge Explorations Botswana Proprietary Limited, 1978; De Beers Prospection Botswana Proprietary Limited, 1996) was used to constrain the depth to bedrock below and near the study area. This was then compared and evaluated against estimates of "Kalahari Sand Thickness" provided by Kolawole et al. (2017) for further validation. A depth to bedrock (i.e., source of the magnetic anomalies) map of the study area was also used as a reference, but due to interference with the Okavango Dike Swarm, its values were considered valid only in specific areas. The depth to bedrock values are calculated using the Source Parameter Imaging (SPI) transformation of the magnetic data (Ojo et al., 2022).

3.2.2 Remote sensing data

Several datasets including satellite images, radar topography, and aeromagnetic data were integrated into the GIS software Global Mapper v15.2 (Blue Marble Geographics, 2011) using an equirectangular projection. Ten Landsat 8 images (with a resolution of 30.0 m/px) acquired in October 2021 (spanning the period in which field work was conducted) were used as the basis for the regional context map (Figure 1B). Elevation data from the Shuttle Radar Topography

Mission (SRTM) (Kobrick, 2006) forms the Digital Elevation Model (DEM; with a resolution of 28.7 m/px) which is presented in a "thermal" color ramp following Crameri et al. (2020) (Figure 4).

The images used to investigate the Martian analog sites included data from the High Resolution Imaging Science Experiment (HiRISE, with a resolution of 0.30 m/px) (McEwen et al., 2007) instrument onboard MRO and the High Resolution Stereo Camera (HRSC, with a resolution of 50.0 m/px) (Neukm and Jaumann, 2004; Jaumann et al., 2007) onboard Mars Express. HiRISE images were processed with the software ISIS 3 (Integrated Software for Imagers and Spectrometers), developed by the USGS (Adoram-Kershner et al., 2020).

Within the GIS environment Surfer® v22 (Golden Software, LLC), we processed aeromagnetic data to create a total magnetic intensity map to further assist in fault identification and ERT survey line placement. A set of NNE-SSW trending magnetic highs were found to be parallel to existing surficial fault scarps, which enabled us to infer the presence of faults that had no obvious surface expression.

4 Results

The faults under investigation are located in the central part of the Ntwetwe Pan and along the western shoreline of the Sua Pan at

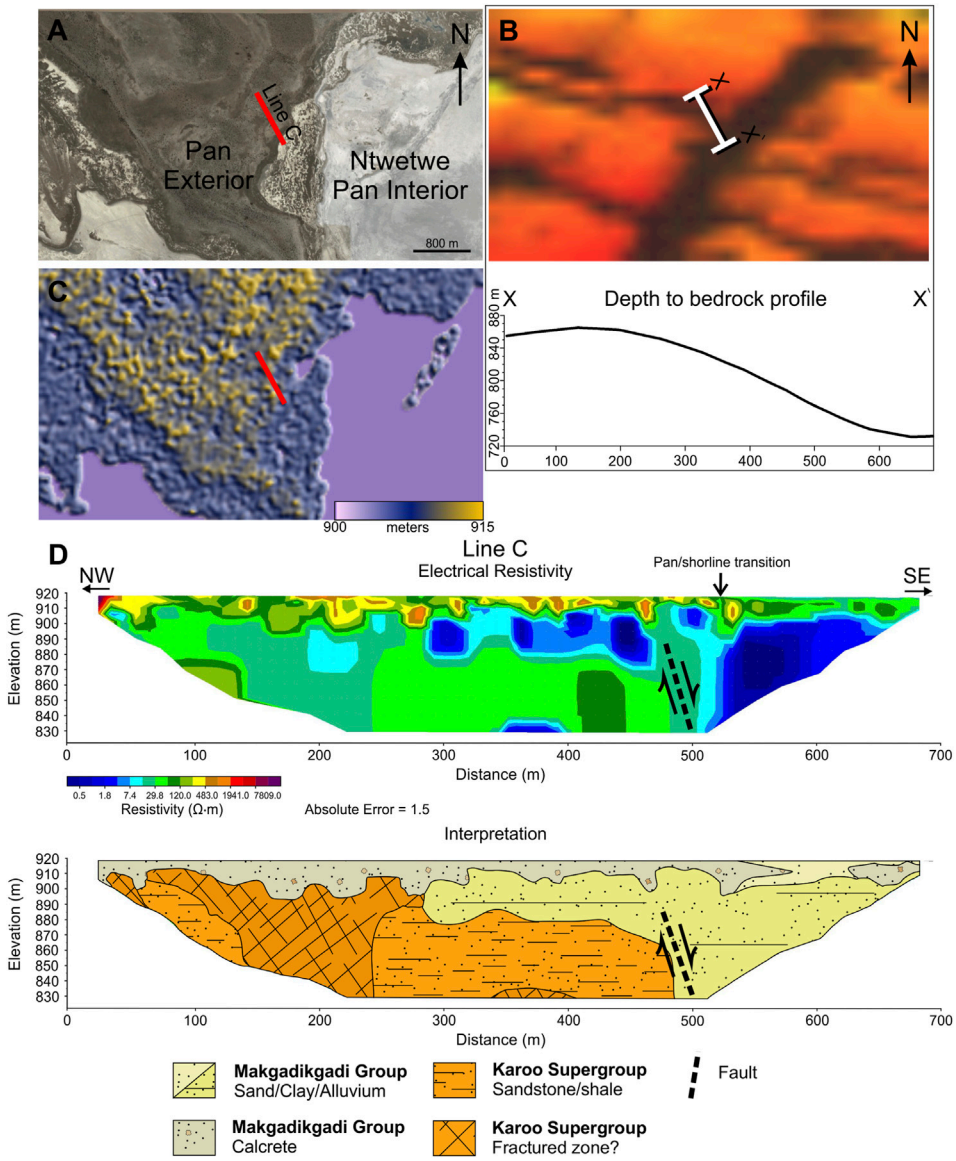

FIGURE 7
(A) Location of ERT survey line C passing across the edge of the shoreline of the Ntwetwe Pan. **(B)** Total magnetic intensity derived from aeromagnetic data. Profile X—X′ shows the depth to bedrock derived from the aeromagnetic data directly where ERT survey line C was placed. Line C is perpendicular to a large northeast-southwest trending structure. The southeast-northwest trending structures are dikes from the Okavango Dike Swarm. **(C)** Surface topography with line C location marked by red line. Note the large difference between the topographic surface change in elevation and the bedrock topography change. **(D)** ERT profile of line C and stratigraphic interpretation. Line C shows the shoreline transition between the pan exterior (NW) and pan interior (SE).

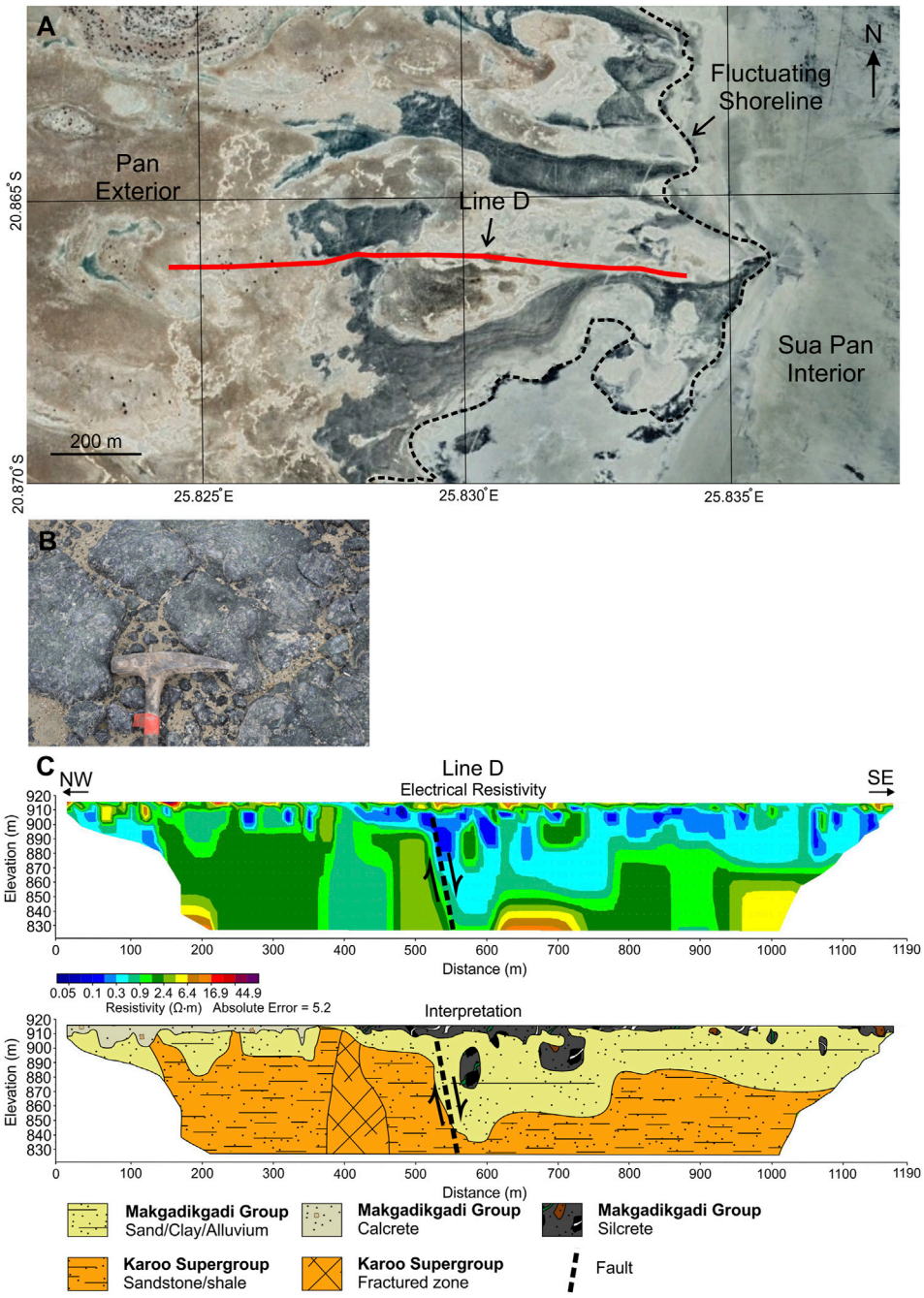

FIGURE 8
(A) Profile of survey line (D). Line D is located at the boundary of the west shoreline of the Sua Pan (dashed black line). Dark material in the Landsat 8 imagery is silcrete (also see Figures 5B, C). **(B)** Example of the silcrete terrain that dominates the western shoreline of the Sua Pan and surroundings of line (D). **(C)** ERT model of line D and stratigraphic interpretation.

an elevation between ca. 908 and 920 m (Figure 3). Lithostratigraphic units identified from the ERT subsurface imaging tended to match with the fault scarp heights previously calculated, as well as the depth to bedrock estimates (Eckardt et al., 2016; Kolawole et al., 2017). These units are referred to as Makgadikgadi Group (referring to sediment infill of the pans) and Karoo Group (referring to bedrock), which include sand, clay, alluvium, sandstone, shale, silcrete, and calcrete (Figure 6; Figure 7; Figure 8).

ERT survey lines A and B are collinear running roughly NE-SW at the center of the Ntwetwe Pan where a major regional fault was inferred to be located (Figure 4, Figure 6A). The distance between lines A and B is wide (approximately 2.8 km) due to caution in the possible existence of two parallel faults (Figure 4). The ground had a rigid and friable salt crust (1–3 cm thick) lying above water-saturated loose sand and clay. These lines revealed a relatively high resistivity top surface (approximately 10–30 m thick), followed by a low resistivity unit (approximately 40–60 m thick),

and further followed by a deeper more resistive unit. This more resistive deep section is the upper surface of a unit whose thickness could not be determined. Two gaps (40 m wide in line A and 80 m wide in line B) were observed in this deep unit and are both located in the positions of the inferred faults. Sections directly above these two gaps have a slightly lower resistivity than the surrounding material.

The faults inferred in the areas of lines A and B were investigated further by imaging where the faults pass from the interior of the Ntwetwe Pan, crossing the Northern shoreline to the exterior of the pan (Figure 3, Figure 7). At this location, the inferred fault trace aligns with a linear magnetic anomaly. The ERT survey line C was placed perpendicular to this linear magnetic anomaly, passing from the edge of the shoreline and across the anomaly (Figure 7A, Figure 6B). The topographic change is less than five m (Figure 7C), whereas the depth to bedrock change across the anomaly is approximately 140 m (Figure 7B). This structure was deemed significant and represents either the same fault (or faults) from lines A and B, a secondary parallel fault, or possibly an infilled fracture related to the fault investigated in lines A and B.

Line C was collected along the main track (a small dirt road which crosses the Ntwetwe Pan in an E-W direction) due to unpredictable conditions driving off-road on the pan sediment in the area (i.e., extremely water saturated top surface). This line was forcibly placed along a particularly hard section characterized by sub-cropping calcretes. Despite this difficulty, 840 m of data were retrieved imaging the transition from the pan floor to the magnetic structure (Figure 7D). This line revealed a more complex subsurface lithiostratigraphy characterized by the high resistivity pan exterior and the low resistivity pan interior. This change is abrupt and is considered to mark the location of a normal fault. A lower resistivity area on the footwall side might indicate a fracture zone.

ERT survey line D was placed perpendicular to the north-south shoreline of the western side of the Sua Pan, which appears to be fault controlled (Schmidt et al., 2023) (Figure 4, Figure 8). Line D is 2.5 km north from Kubu Island, a large ˃60,000 m^2 Archean granite, which was emplaced during the Mesoproterozoic (Majaule et al., 2001). The surface composition of the immediate surroundings of line D is predominately silcrete. The eastern portion of the survey line D ran across a mix of silcrete and loose sediment. In the western 400 m of the line, the surface composition graded into calcrete (similar to that of line C). The lithostratigraphy revealed in line D is characterized by the high resistivity pan exterior and the low resistivity pan interior, and like line C, is an abrupt change considered to mark the location of a normal fault. A lower resistivity area on the footwall side might indicate a fracture zone, and small isolated pockets of high resistivity on the hanging wall side are considered to be silcrete.

5 Discussion

5.1 Faults and water in the Makgadikgadi Pans

ERT survey lines A and B were taken across one of the main northeast-southwest striking faults crossing the Ntwetwe Pan (Figure 6). These survey lines show overall low resistivity values (<1.0 Ω·m) in the very topmost sediments. However, in line A this is only several cm thick and is present only above the inferred fault, whereas in line B it is thicker (1–6 m). This is the saturated sediment of the soft surface of the playa. Both lines A and B show a higher resistivity unit immediately below this (1.0–5.0 Ω·m) in the shallow subsurface that extends from several centimeters to 30 m of thickness in line B. The slightly higher resistivity values may be due to sparse calcrete just below the surface, or a recent deposition that is more sand rich. The thick 40–60 m thick unit which follows has resistivity values of <1.0 Ω·m and is considered to be water saturated sediment. This succession is interpreted to be a mix of sediment, possibly interbedded sand, clays, and alluvium. The lower higher resistivity unit (1.5–6.0 Ω·m) is considered to be the upper surface of the Karoo Supergroup, possibly the sandstones of the Lebung Group (discussion on depth to bedrock interpretation below). The bedrock in line A shows a 40 m wide gap at ca. 450 m from the beginning of the line and a similar 80 m wide gap in line B at ca. 510 m from the beginning of the line. Directly above these two gaps are slightly lower resistivity values and shows tangible evidence for the faults inferred in the airborne geophysics dataset.

The depth to the Karoo Supergroup (i.e., bedrock) presented is one of the few data existing on the real thickness of the Makgadigadi Pans sediment infill. The deepest unit found at an elevation 850 m is interpreted to be the Karoo Supergroup bedrock. Two drill cores (105/17/X015 and 105/17/X016, 10 km apart) located 25 km south of lines A and B, despite being taken from the exterior of the pan, can be used to further constrain the interpretation (De Beers Prospection Botswana Proprietary Limited, 1996). The drill cores have a 1–2 m top section of silcretes and calcretes, followed by a 6–26 m section of sandstones, which together are labeled the Makgadikgadi Group. In drill core 105/17/X015, the Karoo Supergroup immediately follows, alternating between clayey sandstones and siltstones labeled the Mosolotsane Formation (60 m thick), shales labeled the Thabala Formation (40 m thick), and carbonaceous mudstones labeled the Tlapana Formation (80 m thick). At a depth of approximately 209 m a unit of metasediments begins which was interpreted to be older than Karoo. However, drill core 105/17/X016 records only the Tlapana Formation (60 m thick) immediately below the Makgadikgadi Group. None of the four ERT survey lines contained vertical stratigraphic sequences like this which likely means that the unit labeled Makgadikgadi Group in the survey lines (Figure 6, Figure 7, Figure 8) represents the minimum sediment thickness in the center of the pans. Kolawole et al. (2017) proposed that the sediment infill decreased west to east from 150 m thick at the Northwestern side of the Ntwetwe Pan to 30 m thick at the eastern side of the Sua Pan. Specifically, the area of lines A and B was estimated to have an infill thickness of 90–120 m. This estimate matches well with our interpretation of placing the Karoo Supergroup at the bottom of the profiles of lines A and B. Lines C and D image the shoreline and thus it is expected that the Karoo Supergroup would be shallower, as indicated from the drill cores which put the Karoo Supergroup depths at 14–26 m.

The inferred fault from lines A and B was crossed with ERT survey line C where the displacement coincides with the break of the

morphological slope at the surface (approximately 5 m), i.e., the transition between pan surface and shoreline (Figures 7A, C). In fact, at the edge of the shoreline, the depth to bedrock drops 140 m (Figure 7B) and at least 90 m in the ERT survey (Figure 7D). This step matches with the vertical displacement of many of the Makgadikgadi Basin faults measured by Eckardt et al. (2016) and is thus considered to be a normal fault. A wedge of low resistivity (0.0–2.0 Ω·m) just below the surficial calcrete, possibly indicates ingression of pan saline water in the drier shoreline sediments on the hanging wall side (Figure 7D). The high resistivity values of the Karoo Supergroup here (30.0–200 Ω·m) are strikingly apart from the low <1.0 Ω·m values of the sediment infill (i.e. Makgadikgadi Group).

Data from ERT survey line D shows a 20–100 m wide low resistivity area which extends from the surface to at least 100 m in depth. This is possibly a fracture zone associated with a previously proposed fault which coincides with the western shoreline of the Sua Pan (Schmidt et al., 2023). This fault is further attested to by the approximately 50 m vertical offset in the Karoo revealed in the ERT survey. Widespread silcrete directly above this fault might be in part influenced by a shallow aquifer (Lee and Gilkes, 2005) which could utilize faults and fractures zones for fluid movement.

Since we do not see the surface expression of the faults within the pans, it means anytime they have been reactivated, their surface expression is immediately destroyed by flash flooding or buried by new sediment. This could be by repeated and continual seasonal resurfacing. Alternatively, fault activity in these specific areas could be older than the lake and they have been buried by the sediments during the Pleistocene and any significant reactivation (i.e., movement from earthquakes) has not produced a strong surface expression.

5.2 Evaporitic environments and water circulation in the mars equatorial region

The relationship between groundwater upwelling and playa deposits on Earth has the potential to constrain several aspects of evaporitic environments on Mars, including water source, mineral alteration, and the formation of the spring mounds of the ELDs within the Arabia Terra region (Andrews-Hanna et al., 2010; Franchi et al., 2015; Pondrelli et al., 2015; Pondrelli et al., 2019; Pozzobon et al., 2019) and the adjacent Meridiani Planum (Figure 2).

Although this work is not aimed to draw specific comparisons between playa minerals on Earth and Mars, the existence of certain minerals can imply that upwelling groundwater was an active process during their formation. For example, since silcrete contains a significant amount of hydrated silica (Thiry, 1991), opaline deposits identified on the floor of Becquerel crater (Schmidt et al., 2022) could be interpreted as analogues of the duricrust (i.e., silcrete) associated with ERT survey line D at the western shoreline of the Sua Pan (Figures 5B,C, Figure 8B). The clay assembleges adjacent to the large fault in Oyama crater (Loizeau et al., 2012) and in Meridiani Planum (Flahaut et al., 2015) might have been formed in upwelling events (Andrews-Hanna et al., 2007; Andrews-Hanna et al., 2010). Vast assemblages of clays and water-altered minerals are also present in the Makgadikgadi Pans (Shaw et al., 1990; Eckardt et al., 2008; Ringrose et al., 2009). This means that apart from any given pathway for the discharged water, these locations (the pans, Arabia Terra, and Meridiani Planum) are chemically linked.

Buried faults may have contributed to a large percentage of late water activity in Martian history (Pozzobon et al., 2019; Changela et al., 2022; Schmidt et al., 2022). Becquerel crater was proposed to have been influenced by fluid expulsion from buried impact faults and associated fracture zones (Caine et al., 1996; Koeberl et al., 1996; Schmidt et al., 2022) (Figure 2C). Conical layered mounds are a predominant feature in sedimentary deposits in Arabia Terra (e.g. Franchi et al., 2014; Pondrelli et al., 2015; Pozzobon et al., 2019; Annex and Lewis, 2020; Schmidt et al., 2021). These mounds (e.g. Figure 9B) have also been proposed to follow the orientation of buried faults, and could have been formed as spring mounds fed by such faults or at least that there collinear habit is dependent on the presence of faults (Allen and Oehler, 2008; Pozzobon et al., 2019). Clustered or linearly oriented mounds such as these are found in Crommelin, Firsoff, and in particular, Vernal (Schmidt et al., 2021). Nearly identical mounds on the northwestern shoreline of the Ntwetwe Pan (Figure 9A) have been similarly proposed to have been formed by groundwater activity (McFarlane and Long, 2015; Franchi et al., 2020). Becquerel and Danielson craters have observable faulting, albeit in the sedimentary rocks themselves, not the crater floors (Schmidt et al., 2021; Schmidt et al., 2022). Oyama has an obvious wrinkle ridge (deep thrust faults, Mueller and Golombek 2004; Ruj and Kawai 2021) visible from the surface adjacent to layered deposits and hydrated minerals (Loizeau et al., 2012; Loizeau et al., 2015; Schmidt et al., 2021) (Figure 2A). The Meridiani Planum groundwater work of Andrews-Hanna et al. (2007) may indeed be influenced by tectonic faults, ring faults, and/or radial faults (Ormo et al., 2004; Essefi et al., 2014). Furthermore, recent work in Valles Marineris (Gurgurewicz et al., 2022) shows that regional faults have allowed for the fluid migration in deep places like Hebes Chasma. Although Valles Marineris is a much different area, the proof of concept is still present in Arabia Terra and southern edge at Meridiani Planum. It is reasonable to anticipate that Arabia Terra, a highly cratered terrain (Tanaka et al., 2014), would have many faults. Impacts produce radial fault systems, and given that the terrain is also one of the oldest Noachian terrains (Tanaka et al., 2014), there might be relict regional faults possibly formed when Mars was more tectonically active.

Sedimentary sequences within basins and craters in Arabia Terra could exceed several hundred meters, however it is not known for certain the depth of the sedimentary infill in many locations (Franchi et al., 2014; Schmidt et al., 2021). However, Garvin equations and ELD thickness estimates show that buried sediment thickness could exceed 1000 m, whereas here in the pans we propose a thickness of closer to 100 m (Franchi et al., 2014; Pondrelli et al., 2019; Schmidt et al., 2021). Our ERT survey has shown that it is possible that water can be trapped within sediment below a more impermeable unit, which could turn out to be something common within the ELDs. These sedimentary sequences appear to exhibit cyclicity and have been interpreted as a reflection of the alternation of wet and dry conditions,

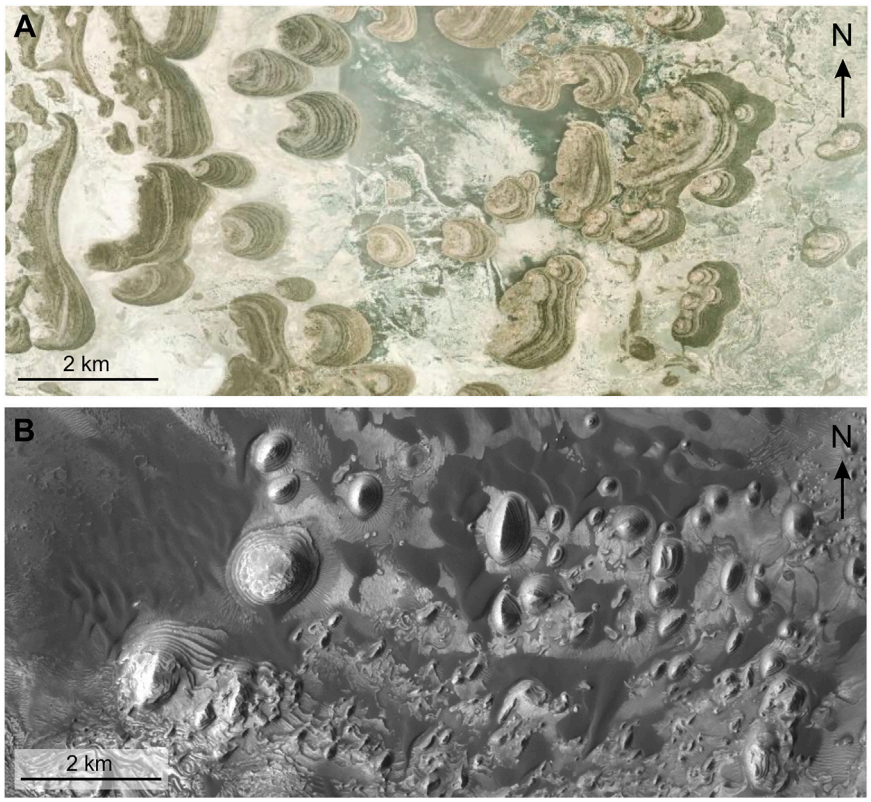

FIGURE 9
A visual comparison of small conical layered mounds in the Ntwetwe Pan (Botswana) and Arabia Terra (Mars). **(A)** Mounds in the Ntwetwe Pan (-20.62, -25.00). **(B)** Mounds in Sera crater Arabia Terra (8.71, -1.08). Sera crater displays layered mounds that are geomorphologically similar to the mounds observed in the Makgadikgadi Pans.

possibly due to fluctuation of the water table (Schmidt et al., 2021; 2022) or obliquity changes (Annex and Lewis, 2020). Thus, there is great potential for the presence of climate change markers hidden within the buried sediment. Markers such as the unconformity in Hebes Chasma (Schmidt et al., 2018) and the marker horizon in Gale Crater (Weitz et al., 2022) may also be present in Arabia Terra, but buried. Such markers could be categorized and linked in order to constrain further the climate change of Mars. Preliminary results from the Radar Imager for Mars Subsurface Experiment (RIMFAX) of the Perseverance rover, despite revealing only 15 m below the surface, shows layering and distinct units on the floor of Jezero crater (Hamran et al., 2022). More intriguing, the 100 m penetration of the Zhurong's Rover Penetrating Radar (RoPeR) shows fining sequences within distinct layered units (Li et al., 2022). This alludes to multiple depositional events and changing energy (i.e. water intensity). Although, these instruments do not involve electrical resistivity, they demonstrate that the value of revealing the subsurface of lacustrine deposits is unquestionable. For these reasons we stress the importance of subsurface imaging instrumentation on future Mars missions, particularly in the proposed sites Oyama, Becquerel, and Meridiani Planum, where the role that faults have had on aqueous environments can be appreciated.

6 Conclusion

We have demonstrated that in an overall arid, windswept environment, groundwater might utilize ancient faults in the bedrock which contribute to the total water entering the basin. Hence, groundwater movement through faults that intersect sediment filled basins and craters on Mars might have had a significant influence on the surface morphology and surface mineralogy identifiable from both orbital and rover datasets.

This work has wide implications for determining how putative water table elevations could have interacted within sediment filled craters on Mars by resolving areas of low resistivity and identifying faults that water could have used as pathways, which is not possible with the current instrumentation present on Mars. Results can also allow us to better infer what the underlying lithology of layered deposits within craters might look like. Furthermore, it demonstrates the scientific importance of future missions to employ subsurface imaging techniques on Mars. The Makgadikgadi Pans show the sedimentary complexity of these environments, not only in subsurface lithostratigraphy, but the types of duricrusts that are likely to be encountered in these playa basins on Mars.

Subsurface imaging will be fundamental in future missions to locating areas of high water saturation on Mars and identifying

buried structures. Missions utilizing drones, as demonstrated by the Ingenuity Mars Helicopter, equipped with a magnetometer would also be extremely beneficial to the location of buried faults (Balaram et al., 2021), as our results in the Makgadikgadi Pans demonstrate. Future field work might include the use of a specific Mars simulant to test the dependability and efficiency of the ERT on Mars (surface terrains more similar to survey lines C and D which were quite dry compared to the interior of the pans). Additionally, the acquisition of deeper penetrating ERT surveys in other areas of the pans where faults are inferred to be (Eckardt et al., 2016; Schmidt et al., 2023), as well as calculating the volume of both annual rainfall and river drainage into the pans and determining the approximate amount of water contained in the pans. In this way, a rough estimate of the amount of groundwater discharged into the pans can be obtained.

Data availability statement

The original contributions presented in the study are included in the article/Supplementary Material, further inquiries can be directed to the corresponding author.

Author contributions

GS: Conceptualization—investigation—writing (original draft)—writing (review and editing)—figures—methodology—supervision. EL: Investigation—writing (original draft). FF: Investigation—writing (original draft)—supervision. AS: Investigation—writing (original draft)—methodology. KH: Investigaion—methodology. FS: Writing (review and editing).

Funding

This research was carried under research permit CMLWS 1/17/4 II (28), granted to FF, by the Ministry of Land Management, Water and Sanitation Services. The field work was funded by Europlanet 2024 RI Transnational Access to GS and EL. Europlanet 2024 RI has received funding from the European Union's Horizon 2020 Research and Innovation Programme under grant agreement number 871149.

Acknowledgments

We would like to thank Estella Atekwana and Folarin Kolawole for advice on faulting and electrical resistivity data interpretation. We also thank Christopher Schmidt for insightful conversations on fault mechanics.

Conflict of interest

The authors declare that the research was conducted in the absence of any commercial or financial relationships that could be construed as a potential conflict of interest.

Publisher's note

References

Abotalib, A. Z., and Heggy, E. (2019). A deep groundwater origin for recurring slope lineae on Mars. *Nat. Geosci.* 12 (4), 235–241. doi:10.1038/s41561-019-0327-5

Achilles, C. N., Rampe, E. B., Downs, R. T., Bristow, T. F., Ming, D. W., Morris, R. V., et al. (2020). Evidence for multiple diagenetic episodes in ancient fluvial-lacustrine sedimentary rocks in Gale crater, Mars. *J. Geophys. Res. Planets* 125 (8), e2019JE006295. doi:10.1029/2019je006295

Adoram-Kershner, L., Berry, K., Lee, K., Laura, J., Mapel, J., Paquette, A., et al. (2020). USGS-Astrogeology/ISIS3: ISIS3.10.1 public release zenodo. Avaliable At: https://github.com/USGS-Astrogeology/ISIS3/tree/3.10.1.

Allen, C. C., and Oehler, D. Z. (2008). A case for ancient springs in Arabia Terra, Mars. *Astrobiology* 8 (6), 1093–1112. doi:10.1089/ast.2008.0239

Al-Samir, M., Nabhan, S., Fritz, J., Winkler, A., Bishop, J. L., Gross, C., and Jaumann, R. (2017). The paleolacustrine evolution of Juventae Chasma and Maja Valles and its implications for the formation of interior layered deposits on Mars. *Icarus*, 292, 125-143. doi:10.1016/j.icarus.2016.12.023

Andrews-Hanna, J. C., Phillips, R. J., and Zuber, M. T. (2007). Meridiani Planum and the global hydrology of Mars. *Nature* 446 (7132), 163–166. doi:10.1038/nature05594

Andrews-Hanna, J. C., Zuber, M. T., Arvidson, R. E., and Wiseman, S. M. (2010). Early Mars hydrology: Meridiani playa deposits and the sedimentary record of Arabia Terra. *J. Geophys. Res. Planets* 115 (E6), E06002. doi:10.1029/2009JE003485

Annex, A. M., and Lewis, K. W. (2020). Regional correlations in the layered deposits of Arabia Terra, Mars. *J. Geophys. Res. Planets* 125 (6), e2019JE006188. doi:10.1029/2019JE006188

Balaram, J., Aung, M., and Golombek, M. P. (2021). The ingenuity helicopter on the perseverance rover. *Space Sci. Rev.* 217 (4), 56–11. doi:10.1007/s11214-021-00815-w

Bierson, C. J., Tulaczyk, S., Courville, S. W., and Putzig, N. E. (2021). Strong MARSIS radar reflections from the base of Martian south polar cap may be due to conductive ice or minerals. *Geophys. Res. Lett.* 48 (13), e2021GL093880. doi:10.1029/2021GL093880

Blue Marble Geographics (2011). *Global mapper*. Hallowell, Maine, USA: Blue Marble Geographics.

Bordy, E. M. (2020). Depositional style changes during the Permo-Carboniferous-early Jurassic evolution of the central Kalahari Karoo sub-Basin, Botswana. *Geol. J.* 55, 5514–5539. doi:10.1002/gj.3751

Burrough, S. L., Thomas, D. S., and Bailey, R. M. (2009). Mega-Lake in the Kalahari: A late Pleistocene record of the palaeolake makgadikgadi system. *Quat. Sci. Rev.* 28 (15-16), 1392–1411. doi:10.1016/j.quascirev.2009.02.007

Cadieux, S. B., and Kah, L. C. (2015). To what extent can intracrater layered deposits that lack clear sedimentary textures be used to infer depositional environments? *Icarus*, 248, 526–538. doi:10.1016/j.icarus.2014.11.004

Caine, J. S., Evans, J. P., and Forster, C. B. (1996). Fault zone architecture and permeability structure. *Geology*, 24(11), 1025–1028. doi:10.1130/0091-7613(1996)024<1025:FZAAPS>2.3.CO;2

Caravaca, G., Le Mouélic, S., Rapin, W., Dromart, G., Gasnault, O., Fau, A., et al. (2021). Long-distance 3D reconstructions using photogrammetry with curiosity's ChemCam remote micro-imager in Gale Crater (Mars). *Remote Sens.* 13 (20), 4068. doi:10.3390/rs13204068

Caravaca, G., Mangold, N., Dehouck, E., Schieber, J., Zaugg, L., Bryk, A. B., et al. (2022). From lake to river: Documenting an environmental transition across the Jura/Knockfarril Hill members boundary in the Glen Torridon region of Gale crater (Mars). *J. Geophys. Res. Planets* 127 (9), e2021JE007093. doi:10.1029/2021JE007093

Carr, M. H., and Head, J. W., III (2010). Geologic history of Mars. *Earth Planet. Sci. Lett.* 294 (3-4), 185–203. doi:10.1016/j.epsl.2009.06.042

Changela, H. G., Chatzitheodoridis, E., Antunes, A., Beaty, D., Bouw, K., Bridges, J. C., et al. (2022). Mars: New insights and unresolved questions–corrigendum. *Int. J. Astrobiol.* 21 (1), 46. doi:10.1017/S1473550421000380

Christensen, P. R., Wyatt, M. B., Glotch, T. D., Rogers, A. D., Anwar, S., Arvidson, R. E., et al. (2004). Mineralogy at Meridiani Planum from the mini-TES experiment on the opportunity rover. *Science* 306 (5702), 1733–1739. doi:10.1126/science.1104909

Crameri, F., Shephard, G. E., and Heron, P. J. (2020). The misuse of colour in science communication. *Nat. Commun.* 11 (1), 5444. doi:10.1038/s41467-020-19160-7

Crowley, J. K. (1993). Mapping playa evaporite minerals with aviris data: A first report from death valley, California. *Remote Sens. Environ.* 44 (2-3), 337–356. doi:10.1016/0034-4257(93)90025-S

Day, M. D., and Catling, D. C. (2020). Potential aeolian deposition of intra-crater layering: A case study of henry crater, Mars. *Bulletin* 132 (3-4), 608–616. doi:10.1130/B35230.1

De Beers Prospection Botswana Proprietary Limited (1996). Final report on prospecting licences 61, 62, 68, 69 and 75/88. *Central and Chobe Districts* 1

deGroot-Hedlin, C., and Constable, S. (1990). Occam's inversion to generate smooth, two-dimensional models from magnetotelluric data. *Geophysics*, 55(12), 1613–1624. doi:10.1190/1.1442813

De Toffoli, B., Mangold, N., Massironi, M., Zanella, A., Pozzobon, R., Le Mouélic, S., et al. (2020). Structural analysis of sulfate vein networks in Gale crater (Mars). *J. Struct. Geol.* 137, 104083. doi:10.1016/j.jsg.2020.104083

Di Achille, G., and Hynek, B. M. (2010). Ancient ocean on Mars supported by global distribution of deltas and valleys. *Nat. Geosci.* 3 (7), 459–463. doi:10.1038/ngeo891

Dickeson, Z. I., and Davis, J. M. (2020). Martian oceans. *Astronomy Geophys.* 61 (3), 311–317. doi:10.1093/astrogeo/ataa038

Dietrich, P., Franchi, F., Setlhabi, L., Prevec, R., and Bamford, M. (2019). The nonglacial diamictite of toutswemogala hill (lower Karoo Supergroup, central Botswana): Implications on the extent of the late paleozoic ice age in the kalahari–karoo basin. *J. Sediment. Res.* 89 (10), 875–889. doi:10.2110/jsr.2019.48

Drake, N. A. (1995). Reflectance spectra of evaporite minerals (400-2500 nm): Applications for remote sensing. *Int. J. Remote Sens.* 16 (14), 2555–2571. doi:10.1080/01431169508954576

Eckardt, F. D., Bryant, R. G., McCulloch, G., Spiro, B., and Woode, W. W. (2008). The hydrochemistry of a semi-arid pan basin case study: Sua Pan, Makgadikgadi, Botswana. *Appl. Geochem.* 23, 1563–1580. doi:10.1016/j.apgeochem.2007.12.033

Eckardt, F. D., Cotterill, F. P., Flügel, T. J., Kahle, B., McFarlane, M., and Rowe, C. (2016). Mapping the surface geomorphology of the makgadikgadi rift zone (MRZ). *Quat. Int.* 404, 115–120. doi:10.1016/j.quaint.2015.09.002

Elburg, M., and Goldberg, A. (2000). Age and geochemistry of Karoo dolerite dykes from northeast Botswana. *J. Afr. Earth Sci.* 31 (3-4), 539–554. doi:10.1016/S0899-5362(00)80006-8

El-Maarry, M. R., Pommerol, A., and Thomas, N. (2013). Analysis of polygonal cracking patterns in chloride-bearing terrains on Mars: Indicators of ancient playa settings. *J. Geophys. Res. Planets* 118 (11), 2263–2278. doi:10.1002/2013JE004463

Essefi, E., Komatsu, G., Fairén, A. G., Chan, M. A., and Yaich, C. (2014). Groundwater influence on the aeolian sequence stratigraphy of the mechertate–chrita–sidi el hani system, Tunisian sahel: Analogies to the wet–dry aeolian sequence stratigraphy at Meridiani Planum, terby crater, and Gale crater, Mars. *Planet. Space Sci.* 95, 56–78. doi:10.1016/j.pss.2013.05.010

Falconbridge Explorations Botswana Proprietary Limited (1978). Final report for state grants 8, 8, 10/77 nata, Sua, dukwe diamond projects central district, Botswana. Bulletin No. 2058.

Farrell, W. Á., Plaut, J. J., Cummer, S. A., Gurnett, D. A., Picardi, G., Watters, T. R., et al. (2009). Is the Martian water table hidden from radar view? *Geophys. Res. Lett.* 36 (15), 38945. doi:10.1029/2009GL038945

Fawdon, P., Balme, M., Davis, J., Bridges, J., Gupta, S., and Quantin-Nataf, C. (2022). Rivers and lakes in Western Arabia Terra: The fluvial catchment of the ExoMars 2022 rover landing site. *J. Geophys. Res. Planets* 127 (2), e2021JE007045. doi:10.1029/2021JE007045

Flahaut, J., Carter, J., Poulet, F., Bibring, J. P., Van Westrenen, W., Davies, G. R., et al. (2015). Embedded clays and sulfates in Meridiani Planum, Mars. *Icarus* 248, 269–288. doi:10.1016/j.icarus.2014.10.046

Flahaut, J., Martinot, M., Bishop, J. L., Davies, G. R., and Potts, N. J. (2017). Remote sensing and *in situ* mineralogic survey of the Chilean salars: An analog to Mars evaporate deposits? *Icarus* 282, 152–173. doi:10.1016/j.icarus.2016.09.041

Franchi, F., Cavalazzi, B., Evans, M., Filippidou, S., Mackay, R., Malaspina, P., et al. (2022). Late pleistocene–holocene palaeoenvironmental evolution of the Makgadikgadi Basin, central Kalahari, Botswana: New evidence from shallow sediments and ostracod fauna. *Front. Ecol. Evol.* 10, 818417. doi:10.3389/fevo.2022.818417

Franchi, F., Kelepile, T., Di Capua, A., De Wit, M. C., Kemiso, O., Lasarwe, R., et al. (2021). Lithostratigraphy, sedimentary petrography and geochemistry of the upper Karoo Supergroup in the central Kalahari Karoo sub-basin, Botswana. *J. Afr. Earth Sci.* 173, 104025. doi:10.1016/j.jafrearsci.2020.104025

Franchi, F., MacKay, R., Selepeng, A. T., and Barbieri, R. (2020). Layered mound, inverted channels and polygonal fractures from the Makgadikgadi pan (Botswana): Possible analogues for Martian aqueous morphologies. *Planet. Space Sci.* 192, 105048. doi:10.1016/j.pss.2020.105048

Franchi, F., Rossi, A. P., Pondrelli, M., and Cavalazzi, B. (2014). Geometry, stratigraphy and evidences for fluid expulsion within Crommelin crater deposits, Arabia Terra, Mars. *Planet. Space Sci.* 92, 34–48. doi:10.1016/j.pss.2013.12.013

Fueten, F., Stesky, R. M., and MacKinnon, P. (2005). Structural attitudes of large scale layering in Valles Marineris, Mars, calculated from Mars orbiter laser altimeter data and Mars orbiter camera imagery. *Icarus* 175 (1), 68–77. doi:10.1016/j.icarus.2004.11.010

Grey, D. R. C., and Cooke, H. J. (1977). Some problems in the Quaternary evolution of the landforms of northern Botswana. *Catena* 4 (1-2), 123–133. doi:10.1016/0341-8162(77)90014-5

Grotzinger, J. P., Arvidson, R. E., Bell, J. F., Iii, Calvin, W., Clark, B. C., Fike, D. A., et al. (2005). Stratigraphy and sedimentology of a dry to wet eolian depositional system, Burns formation, Meridiani Planum, Mars. *Earth Planet. Sci. Lett.* 240 (1), 11–72. doi:10.1016/j.epsl.2005.09.039

Gurgurewicz, J., Mège, D., Schmidt, F., Douté, S., and Langlais, B. (2022). Megashears and hydrothermalism at the martian crustal dichotomy in Valles Marineris. *Commun. Earth Environ.* 3 (1), 282. doi:10.1038/s43247-022-00612-5

Haddon, I. G., and McCarthy, T. S. (2005). The mesozoic–cenozoic interior sag basins of central Africa: The late-cretaceous–Cenozoic Kalahari and Okavango basins. *J. Afr. Earth Sci.* 43 (1-3), 316–333. doi:10.1016/j.jafrearsci.2005.07.008

Hamran, S. E., Paige, D. A., Allwood, A., Amundsen, H. E., Berger, T., Brovoll, S., et al. (2022). Ground penetrating radar observations of subsurface structures in the floor of Jezero crater, Mars. *Sci. Adv.* 8 (34), eabp8564. doi:10.1126/sciadv.abp8564

Haskin, L. A., Wang, A., Jolliff, B. L., McSween, H. Y., Clark, B. C., Des Marais, D. J., et al. (2005). Water alteration of rocks and soils on Mars at the Spirit rover site in Gusev crater. *Nature* 436 (7047), 66–69. doi:10.1038/nature03640

Hurowitz, J. A., Grotzinger, J. P., Fischer, W. W., McLennan, S. M., Milliken, R. E., Stein, N., et al. (2017). Redox stratification of an ancient lake in Gale crater, Mars. *Science* 356 (6341), eaah6849. doi:10.1126/science.aah6849

Jaumann, R., Neukum, G., Behnke, T., Duxbury, T. C., Eichentopf, K., Flohrer, J., et al.HRSC Co-Investigator Team (2007). The high-resolution stereo camera (HRSC) experiment on Mars Express: Instrument aspects and experiment conduct from interplanetary cruise through the nominal mission. *Planet. Space Sci.* 55 (7-8), 928–952. doi:10.1016/j.pss.2006.12.003

Jordan, R., Picardi, G., Plaut, J., Wheeler, K., Kirchner, D., Safaeinili, A., et al. (2009). The Mars express MARSIS sounder instrument. *Planet. Space Sci.* 57 (14-15), 1975–1986. doi:10.1016/j.pss.2009.09.016

Kah, L. C., Stack, K. M., Eigenbrode, J. L., Yingst, R. A., and Edgett, K. S. (2018). Syndepositional precipitation of calcium sulfate in Gale Crater, Mars. *Terra nova.* 30 (6), 431–439. doi:10.1111/ter.12359

Kinabo, B. D., Atekwana, E. A., Hogan, J. P., Modisi, M. P., Wheaton, D. D., and Kampunzu, A. B. (2007). Early structural development of the Okavango rift zone, NW Botswana. *J. Afr. Earth Sci.* 48 (2-3), 125–136. doi:10.1016/j.jafrearsci.2007.02.005

Kobrick, M. (2006). On the toes of giants-How SRTM was born. *Photogrammetric Eng. Remote Sens.* 72 (3), 206–210.

Koeberl, C., Reimold, W. U., and Brandi, D. (1996). Red Wing Creek structure, North Dakota: Petrographical and geochemical studies, and confirmation of impact origin. *Meteorit. Planet. Sci.* 31 (3), 335–342. doi:10.1111/j.1945-5100.1996.tb02070.x

Kolawole, F., Atekwana, E. A., Laó-Dávila, D. A., Abdelsalam, M. G., Chindandali, P. R., Salima, J., et al. (2018). High-resolution electrical resistivity and aeromagnetic imaging reveal the causative fault of the 2009 M w 6.0 Karonga, Malawi earthquake. *Geophys. J. Int.* 213 (2), 1412–1425. doi:10.1093/gji/ggy066

Kolawole, F., Atekwana, E. A., Malloy, S., Stamps, D. S., Grandin, R., Abdelsalam, M. G., et al. (2017). Aeromagnetic, gravity, and Differential Interferometric Synthetic Aperture Radar analyses reveal the causative fault of the 3 April 2017M_w6.5 Moiyabana, Botswana, earthquake. *Geophys. Res. Lett.* 44 (17), 8837–8846. doi:10.1002/2017gl074620

Le Deit, L., Hauber, E., Fueten, F., Pondrelli, M., Rossi, A. P., and Jaumann, R. (2013). Sequence of infilling events in Gale Crater, Mars: Results from morphology, stratigraphy, and mineralogy. *J. Geophys. Res. Planets* 118 (12), 2439–2473. doi:10.1002/2012JE004322

Le Deit, L., Mangold, N., Forni, O., Cousin, A., Lasue, J., Schröder, S., et al. (2016). The potassic sedimentary rocks in Gale Crater, Mars, as seen by ChemCam on board Curiosity. *J. Geophys. Res. Planets* 121 (5), 784–804. doi:10.1002/2015JE004987

Leask, E. K., and Ehlmann, B. L. (2022). Evidence for deposition of chloride on Mars from small-volume surface water events into the Late Hesperian-Early Amazonian. *AGU Adv.* 3 (1), e2021AV000534. doi:10.1029/2021av000534

Lee, S. Y., and Gilkes, R. J. (2005). Groundwater geochemistry and composition of hardpans in southwestern Australian regolith. *Geoderma*, 126 (1-2), 59-84. doi:10.1016/j.geoderma.2004.11.007

Lekula, M., Lubczynski, M. W., and Shemang, E. M. (2018). Hydrogeological conceptual model of large and complex sedimentary aquifer systems–Central Kalahari Basin. *Phys. Chem. Earth, Parts A/B/C* 106, 47–62. doi:10.1016/j.pce.2018.05.006

Li, C., Zheng, Y., Wang, X., Zhang, J., Wang, Y., Chen, L., et al. (2022). Layered subsurface in utopia Basin of Mars revealed by Zhurong rover radar. *Nature* 610 (7931), 308–312. doi:10.1038/s41586-022-05147-5

Loizeau, D., Mangold, N., Poulet, F., Bibring, J. P., Bishop, J. L., Michalski, J., et al. (2015). History of the clay-rich unit at Mawrth Vallis, Mars: High-resolution mapping of a candidate landing site. *J. Geophys. Res. Planets* 120 (11), 1820–1846. doi:10.1002/2015JE004894

Loizeau, D., Werner, S. C., Mangold, N., Bibring, J. P., and Vago, J. L. (2012). Chronology of deposition and alteration in the mawrth vallis region, Mars. *Planet. Space Sci.* 72 (1), 31–43. doi:10.1016/j.pss.2012.06.023

Loke, M. H., and Barker, R. D. (1996). Rapid least-squares inversion of apparent resistivity pseudo sections by a quasi-Newton method. *Geophys. Prospect.* 44, 131–152. doi:10.1111/j.1365-2478.1996.tb00142.x

Loke, M. H. (2001). Electrical imaging surveys for environmental and engineering studies: A practical guide to 2D and 3D surveys. Available at: http://www.geotomosoft.com/downloads.php.

Lucchitta, B. K. (2010). *Lakes on Mars [book]*. edited by N. A. Cabrol and E. A. Grin, pp. 111, Amsterdam: Elsevier.

Lucchitta, B. K., Isbell, N. K., and Howington-Kraus, A. (1994). Topography of Valles Marineris: Implications for erosional and structural history. *J. Geophys. Res. Planets* 99 (E2), 3783–3798. doi:10.1029/93JE03095

Majaule, T., Hanson, R. E., Key, R. M., Singletary, S. J., Martin, M. W., and Bowring, S. A. (2001). The magondi belt in northeast Botswana: Regional relations and new geochronological data from the Sua Pan area. *J. Afr. Earth Sci.* 32 (2), 257–267. doi:10.1016/S0899-5362(01)90006-5

Mangold, N., Gupta, S., Gasnault, O., Dromart, G., Tarnas, J. D., Sholes, S. F., et al. (2021). Perseverance rover reveals an ancient delta-lake system and flood deposits at Jezero crater, Mars. *Science* 374 (6568), 711–717. doi:10.1126/science.abl4051

McCulloch, G. M., Irvine, K., Eckardt, F. D., and Bryant, R. (2008). Hydrochemical fluctuations and crustacean community composition in an ephemeral saline lake (Sua Pan, Makgadikgadi Botswana). *Hydrobiologia* 596, 31–46. doi:10.1007/s10750-007-9055-8

McEwen, A. S., Eliason, E. M., Bergstrom, J. W., Bridges, N. T., Hansen, C. J., Delamere, W. A., et al. (2007). Mars reconnaissance orbiter's high resolution imaging science experiment (HiRISE). *J. Geophys. Res.* 112, E05s02. doi:10.1029/2005je002605

McFarlane, M. J., and Long, C. W. (2015). Pan floor 'barchan'mounds, Ntwetwe Pan, Makgadikgadi, Botswana: Their origin and palaeoclimatic implications. *Quat. Int.* 372, 108–119. doi:10.1016/j.quaint.2014.10.008

McKenna, O. P., and Sala, O. E. (2018). Groundwater recharge in desert playas: Current rates and future effects of climate change. *Environ. Res. Lett.* 13 (1), 014025. doi:10.1088/1748-9326/aa9eb6

Michalski, J. R., Goudge, T. A., Crowe, S. A., Cuadros, J., Mustard, J. F., and Johnson, S. S. (2022). Geological diversity and microbiological potential of lakes on Mars. *Nat. Astron.* 6, 1133–1141. doi:10.1038/s41550-022-01743-7

Modisi, M. P., Atekwana, E. A., Kapunzu, A. B., and Mgwisanyi, T. H. (2000). Rift kinematics during the incipient stages of continental fragmentation: Evidence from the nascent Okavango rift, northwest Botswana. *Geology* 28, 939–942. doi:10.1130/0091-7613(2000)28<939:RKDTIS>2.0.CO;2

Moore, A. E., Cotterill, F. P. D., and Eckardt, F. D. (2012). The evolution and ages of makgadikgadi palaeo-lakes: Consilient evidence from Kalahari drainage evolution south-central Africa. *South Afr. J. Geol.* 115 (3), 385–413. doi:10.2113/gssajg.115.3.385

Mueller, K., and Golombek, M. (2004). Compressional structures on Mars. *Annu. Rev. Earth Planet. Sci.* 32, 435–464. doi:10.1146/annurev.earth.32.101802.120553

Mukul, M., Srivastava, V., Jade, S., and Mukul, M. (2017). Uncertainties in the shuttle radar topography mission (SRTM) heights: Insights from the indian himalaya and peninsula. *Sci. Rep.* 7 (1), 41672–41710. doi:10.1038/srep41672

Nachon, M., Clegg, S. M., Mangold, N., Schröder, S., Kah, L. C., Dromart, G., et al. (2014). Calcium sulfate veins characterized by ChemCam/Curiosity at Gale crater, Mars. *J. Geophys. Res. Planets* 119 (9), 1991–2016. doi:10.1002/2013je004588

Nash, D. J., Thomas, D. S., and Shaw, P. A. (1994). Siliceous duricrusts as palaeoclimatic indicators: Evidence from the Kalahari desert of Botswana. *Palaeogeogr. Palaeoclimatol. Palaeoecol.* 112 (3-4), 279–295. doi:10.1016/0031-0182(94)90077-9

Neukum, G., and Jaumann, R. (2004). Hrsc: The high resolution stereo camera of Mars Express. *Mars Express Sci. Payload* 1240, 17–35.

Nield, J. M., Wiggs, G. F. S., King, J., Bryant, R. G., Eckardt, F. D., Thomas, D. S. G., et al. (2016). Climate–surface–pore-water interactions on a salt crusted playa: Implications for crust pattern and surface roughness development measured using terrestrial laser scanning. *Earth Surf. Process. Landforms* 41, 738–753. doi:10.1002/esp.3860

Nunes, D. C., Smrekar, S. E., Safaeinili, A., Holt, J., Phillips, R. J., Seu, R., et al. (2010). Examination of gully sites on Mars with the shallow radar. *J. Geophys. Res. Planets* 115 (E10), E10004. doi:10.1029/2009JE003509

Ojo, O. O., Ohenhen, L. O., Kolawole, F., Johnson, S. G., Chindandali, P. R., Atekwana, E. A., et al. (2022). Under-displaced normal faults: Strain accommodation along an early-stage rift-bounding fault in the Southern Malawi Rift. *Front. Earth Sci.* 10, 846389. doi:10.3389/feart.2022.846389

Ormö, J., Komatsu, G., Chan, M. A., Beitler, B., and Parry, W. T. (2004). Geological features indicative of processes related to the hematite Formation in Meridiani Planum and aram chaos, Mars: A comparison with diagenetic hematite deposits in southern Utah, USA. *Icarus* 171 (2), 295–316. doi:10.1016/j.icarus.2004.06.001

Orofino, V., Alemanno, G., Di Achille, G., and Mancarella, F. (2018). Estimate of the water flow duration in large Martian fluvial systems. *Planet. Space Sci.* 163, 83–96. doi:10.1016/j.pss.2018.06.001

Orosei, R., Lauro, S. E., Pettinelli, E., Cicchetti, A. N. D. R. E. A., Coradini, M., Cosciotti, B., et al. (2018). Radar evidence of subglacial liquid water on Mars. *Science* 361 (6401), 490–493. doi:10.1126/science.aar7268

Podgorski, J. E., Green, A. G., Kgotlhang, L., Kinzelbach, W. K., Kalscheuer, T., Auken, E., et al. (2013). Paleo-megalake and paleo-megafan in southern Africa. *Geology* 41 (11), 1155–1158. doi:10.1130/G34735.1

Pondrelli, M., Rossi, A. P., Le Deit, L., Fueten, F., van Gasselt, S., Glamoclija, M., et al. (2015). Equatorial layered deposits in Arabia Terra, Mars: Facies and process variability. *Bulletin* 127 (7-8), 1064–1089. doi:10.1130/B31225.1

Pondrelli, M., Rossi, A. P., Le Deit, L., Schmidt, G. W., Pozzobon, R., Hauber, E., et al. (2019). Groundwater control and process variability on the equatorial layered deposits of kotido crater, Mars. *J. Geophys. Res. Planets* 124, 779–800. doi:10.1029/2018JE005656

Pondrelli, M., Rossi, A. P., Marinangeli, L., Hauber, E., Gwinner, K., Baliva, A., et al. (2008). Evolution and depositional environments of the Eberswalde fan delta, Mars. *Icarus* 197 (2), 429–451. doi:10.1016/j.icarus.2008.05.018

Pozzobon, R., Mazzarini, F., Massironi, M., Rossi, A. P., Pondrelli, M., Cremonese, G., et al. (2019). Fluids mobilization in Arabia Terra, Mars: Depth of pressurized reservoir from mounds self-similar clustering. *Icarus* 321, 938–959. doi:10.1016/j.icarus.2018.12.023

Rapin, W., Meslin, P. Y., Maurice, S., Vaniman, D., Nachon, M., Mangold, N., et al. (2016). Hydration state of calcium sulfates in Gale crater, Mars: Identification of bassanite veins. *Earth Planet. Sci. Lett.* 452, 197–205. doi:10.1016/j.epsl.2016.07.045

Richards, J., Burrough, S., Wiggs, G., Hills, T., Thomas, D., and Moseki, M. (2021). Uneven surface moisture as a driver of dune formation on ephemeral lake beds under conditions similar to the present day: A model-based assessment from the Makgadikgadi Basin, northern Botswana. *Earth Surf. Proc. Land.* 46, 3078–3095. doi:10.1002/esp.5215

Riedel, F., Henderson, A. C. G., Heußner, K. U., Kaufmann, G., Kossler, A., Leipe, C., et al. (2014). Dynamics of a Kalahari long-lived mega-lake system—Hydromorphological and limnological changes in the Makgadikgadi Basin (Botswana) during the terminal 50 ka. *Hydrobiologia* 739, 25–53. doi:10.1007/s10750-013-1647-x

Ringrose, S., Harris, C., Huntsman-Mapila, P., Vink, B. W., Diskins, S., Vanderpost, C., et al. (2009). Origins of strandline duricrusts around the Makgadikgadi Pans (Botswana Kalahari) as deduced from their chemical and isotope composition. *Sediment. Geol.* 219 (1-4), 262–279. doi:10.1016/j.sedgeo.2009.05.021

Rossi, A. P., Neukum, G., Pondrelli, M., Van Gasselt, S., Zegers, T., Hauber, E., et al. (2008). Large-scale spring deposits on Mars? *J. Geophys. Res.* 113. doi:10.1029/2007JE003062

Ruj, T., and Kawai, K. (2021). A global investigation of wrinkle ridge formation events; implications towards the thermal evolution of Mars. *Icarus* 369, 114625. doi:10.1016/j.icarus.2021.114625

Salese, F., McMahon, W. J., Balme, M. R., Ansan, V., Davis, J. M., and Kleinhans, M. G. (2020). Sustained fluvial deposition recorded in Mars' Noachian stratigraphic record. *Nat. Commun.* 11 (1), 2067. doi:10.1038/s41467-020-15622-0

Salese, F., Pondrelli, M., Neeseman, A., Schmidt, G., and Ori, G. G. (2019). Geological evidence of planet-wide groundwater system on Mars. *J. Geophys. Res. Planets* 124 (2), 374–395. doi:10.1029/2018JE005802

Schmidt, G., Franchi, F., Salvini, F., Selepeng, A. T., Luzzi, E., Schmidt, C., et al. (2023). Fault controlled geometries by inherited tectonic texture at the southern end of the East African Rift System in the Makgadikgadi Basin, northeastern Botswana. *Tectonophysics* 846, 229678. doi:10.1016/j.tecto.2022.229678

Schmidt, G., Fueten, F., Stesky, R., Flahaut, J., and Hauber, E. (2018). Geology of Hebes Chasma, Mars: 1. Structure, stratigraphy, and mineralogy of the interior layered deposits. *J. Geophys. Res. Planets* 123 (11), 2893–2919. doi:10.1029/2018JE005658

Schmidt, G., Luzzi, E., Rossi, A. P., Pondrelli, M., Apuzzo, A., and Salvini, F. (2022). Protracted hydrogeological activity in Arabia Terra, Mars: Evidence from the structure and mineralogy of the layered deposits of Becquerel crater. *J. Geophys. Res. Planets* 127 (9), e2022JE007320. doi:10.1029/2022JE007320

Schmidt, G., Pondrelli, M., Salese, F., Rossi, A. P., Le Deit, L., Fueten, F., et al. (2021). Depositional controls of the layered deposits of Arabia Terra, Mars: Hints from basin geometries and stratigraphic trends. *J. Geophys. Res. Planets* 126 (11), e2021JE006974. doi:10.1029/2021JE006974

Schmidt, M., Fuchs, M., Henderson, A. C. G., Kossler, A., Leng, M. J., Mackay, A. W., et al. (2017). Paleolimnological features of a mega-lake phase in the Makgadikgadi Basin (Kalahari, Botswana) during marine isotope stage 5 inferred from diatoms. *J. Paleolimnol.* 58, 373–390. doi:10.1007/s10933-017-9984-9

Seu, R., Phillips, R. J., Biccari, D., Orosei, R., Masdea, A., Picardi, G., et al. (2007). SHARAD sounding radar on the Mars Reconnaissance Orbiter. *J. Geophys. Res. Planets*, 112 (E5). doi:10.1029/2006JE002745

Shaw, P. A., Cooke, H. J., and Perry, C. C. (1990). Microbialitic silcretes in highly alkaline environments: Some observations from Sua Pan, Botswana. *South Afr. J. Geol.* 93 (4), 803–808.

Sori, M. M., and Bramson, A. M. (2019). Water on Mars, with a grain of salt: Local heat anomalies are required for basal melting of ice at the south pole today. *Geophys. Res. Lett.* 46 (3), 1222–1231. doi:10.1029/2018GL080985

Squyres, S. W., Arvidson, R. E., Bell, J. F., Iii, Bruckner, J., Cabrol, N. A., Calvin, W., et al. (2004). The opportunity rover's Athena science investigation at Meridiani Planum, Mars. *science* 306 (5702), 1698–1703. doi:10.1126/science.1106171

Stein, N., Grotzinger, J. P., Schieber, J., Mangold, N., Hallet, B., Newsom, H., et al. (2018). Desiccation cracks provide evidence of lake drying on Mars, Sutton Island member, Murray formation, Gale Crater. *Geology* 46 (6), 515–518. doi:10.1130/G40005.1

Sudha, K., Israil, M., Mittal, S., and Rai, J. (2009). Soil characterization using electrical resistivity tomography and geotechnical investigations. *J. Appl. Geophys.* 67 (1), 74–79. doi:10.1016/j.jappgeo.2008.09.012

Tanaka, K. L., Skinner, J. A., Jr, Dohm, J. M., Irwin, R. P., III, Kolb, E. J., Fortezzo, C. M., et al. (2014). *Geologic map of Mars: U.S. Geological Survey Scientific Investigations Map 3292, scale 1:20,000,000, pamphlet 43 p.* doi:10.3133/sim3292

Thiry, M. (1991). Pedogenic and groundwater silcretes at Stuart Creek opal field, South Australia. *J. Sediment. Res.* 61 (1), 111–127. doi:10.1306/D426769F-2B26-11D7-8648000102C1865D

Thomas, D., and Shaw, P. A. (1991). *The Kalahari environment*. Cambridge, UK: Cambridge University Press.

Viviano, C. E., Seelos, F. P., Murchie, S. L., Kahn, E. G., Seelos, K. D., Taylor, H. W., et al. (2014). Revised CRISM spectral parameters and summary products based on the currently detected mineral diversity on Mars. *J. Geophys. Res. Planets* 119 (6), 1403–1431. doi:10.1002/2014JE004627

Wang, A., Jolliff, B. L., Liu, Y., and Connor, K. (2016). Setting constraints on the nature and origin of the two major hydrous sulfates on Mars: Monohydrated and polyhydrated sulfates. *J. Geophys. Res.: Planets*, 121(4), 678-694. doi:10.1002/2015JE004889

Weitz, C. M., Lewis, K. W., Bishop, J. L., Thomson, B. J., Arvidson, R. E., Grant, J. A., et al. (2022). Orbital observations of a marker horizon at GALE CRATER. *J. Geophys. Res. Planets* 127, e2022JE007211. doi:10.1029/2022JE007211

Zurek, R. W., and Smrekar, S. E. (2007). An overview of the Mars Reconnaissance Orbiter (MRO) science mission. *J. Geophys. Res. Planets*, 112 (E5). doi:10.1029/2006JE002701